Atmospheric Research 271 (2022) 106100

Contents lists available at ScienceDirect

Atmospheric Research

journal homepage: www.elsevier.com/locate/atmosres

Distribution and sources of SVOCs in fine and coarse aerosols in the megacity of Istanbul

Rosa M. Flores [a,*], Hüseyin Özdemir [b], Alper Ünal [c], Mete Tayanç [a]

[a] Marmara University, Department of Environmental Engineering, 34722 Istanbul, Turkey
[b] Bahcesehir University, Department of Civil Engineering, 34353 Istanbul, Turkey
[c] Istanbul Technical University, Eurasia Institute of Earth Sciences, 34469 Istanbul, Turkey

ARTICLE INFO

Keywords:
Diagnostic ratios
Megacity
N-alkanes
PCA
PAH
Size distribution

ABSTRACT

Approximately 15.4 million people are continuously exposed to various air pollutants in the megacity of Istanbul. Anthropogenic activities in Istanbul generate emissions from mobile sources (i.e., vehicles, aircraft, ships, etc.) and stationary sources such as industrial and residential heating emissions. Biogenic emissions and long-range transport such as desert dust from Sahara and pollutants from Balkan countries also contribute to the local air pollution in Istanbul. In this work, fine ($D_p < 2.5$ μm) and coarse ($D_p > 2.5$ μm) particles were collected with a high-volume sampler during four seasons of the period Jan 2017 - Jan 2018. A total of 15 PAHs and 28 *n*-alkanes were identified and quantified with a newly developed thermal desorption – gas chromatography with mass spectrometry method (TD-GC–MS). Source analysis was performed with PAH and *n*-alkane diagnostic ratios, and source apportionment was performed with principal component analysis. The yearly averages of PAHs and *n*-alkanes in the fine fraction were 21.6 ng m^{-3} and 103.8 ng m^{-3}, with daily averages of 7.1–80.8 ng m^{-3} and 55.3–204.2 ng m^{-3}, respectively. Approximately 90% of the PAHs and *n*-alkanes were found in the fine PM fraction in this traffic site. The BaP carcinogenic (BaP-TEQ) and mutagenic (BaP-MEQ) equivalents were on average 5.47 ± 0.64 and 4.72 ± 0.8 ng m^{-3} in the fine fraction, respectively, and were approximately 6–7 times lower in the coarse fraction. This has important implications due to the respirable nature of fine aerosols and their longer lifetimes in the atmosphere. Multivariate analysis coupled with principal component analysis led to an important result that the organic aerosol mainly originates from two local sources: road traffic (50.4%) and shipping emissions (26.6%). The results found in this work indicate the urgent need for the application of mitigation measures to control road traffic and minimize the emissions from ships passing through the İstanbul Bosphorus.

1. Introduction

In densely populated cities, mobile emissions constitute the major source of air pollutants that have detrimental effects on human health. The transportation sector is responsible for large emissions of organic aerosol, black carbon, and gases such as CO, CO_2, NO_x, and VOCs. Organic aerosol (OA), both primary (POA) and secondary (SOA), comprises a large fraction of fine particulate matter in the urban atmosphere (Molina, 2021). The abundance and chemical composition of OA vary temporally and geographically according to changes in emission sources, physicochemical properties, atmospheric transport, dispersion, transformation, and removal processes (An et al., 2019). Organic aerosol is composed of a complex mixture of species with various ranges of volatilities such as intermediate volatility organic compounds (IVOCs), semi-volatile organic compounds (SVOCs), low-volatility organic compounds (LVOCs), and extremely low volatility organic compounds (ELVOCs).

Intermediate-volatility and semi-volatile organic compounds (I/SVOCs) may be emitted in the gas- and particle- phases and when emitted in the gas phase, may partition into the particle phase at ambient temperature (Liu et al., 2021). These I/SVOCs are important precursors to ozone formation and SOA production. A large fraction (i,e., 50–86%) of SOA is produced from the oxidation of IVOCs and SVOCs in megacities (Khare et al., 2020; Li et al., 2020; Ma et al., 2017). However, IVOCs and SVOCs have not been completely characterized in field measurements, particularly at urban traffic sites (Liu et al., 2021). On-

* Corresponding author.
E-mail address: rflores@marmara.edu.tr (R.M. Flores).

https://doi.org/10.1016/j.atmosres.2022.106100
Received 3 January 2022; Received in revised form 17 February 2022; Accepted 20 February 2022
Available online 24 February 2022

road vehicles are an important source of I/SVOCs in urban areas. It has been recently estimated that diesel vehicles have emission factors 15 times higher than gasoline vehicles (Tang et al., 2021).

Alkanes and polycyclic aromatic hydrocarbons (PAHs) are of special importance due to their large emissions from anthropogenic sources, particularly from on-road vehicles, and carcinogenic effects, respectively (Lambe et al., 2012; Li et al., 2021; Masiol et al., 2012). The carcinogenic effects of PAHs depend on the phase that enters the body (i.e., gas or particle). Long-term effects are observed when the PAH enters the lung in the particle phase (Hussain et al., 2018; Pandey et al., 2013). Although low molecular weight (LMW) PAHs are the most abundant in the urban atmosphere, they have weaker carcinogenic/mutagenic properties since the carcinogenic effects increase with molecular weight (Pandey et al., 2013; Yang et al., 2021). Furthermore, PAHs can react with ozone (O_3) and nitrogen oxides (NO_x) to produce derivatives with low vapor pressures that may predominantly occur in the particle phase (Yang et al., 2021). The production of SOA in chemical models has a poor agreement with field measurements. The high uncertainty of the model forecasts is mainly due to a lack of understanding of the chemical characterization of SOA precursors, their sources, and their diurnal and seasonal variations (Flores and Doskey, 2021; Khare and Gentner, 2018).

The main purpose of this work is to study the daily and seasonal variations of *n*-alkanes and PAHs in fine and coarse particulate matter (PM) fractions for the first time in the megacity of Istanbul. To accomplish this, 300 fine and 50 coarse PM samples were collected at one of the busiest districts of Istanbul, Beşiktaş, and analyzed for identification, and quantification of 16 PAHs and 28 *n*-alkane species. Possible sources and their variability with meteorological conditions were also investigated. In Istanbul, one study reported PAHs in total suspended particles (TSP) in fall and winter 2007 (Hanedar et al., 2011) and another study reported the levels of PAHs in TSP during a two-week winter period with high pollution levels (Kuzu et al., 2021). To the best of our knowledge, our manuscript provides the first investigation of the daily and seasonal variations of PAHs and *n*-alkanes in fine and coarse PM size fractions, as well as source analysis and apportionment.

2. Experimental

2.1. Site description and collection of fine and coarse particulate matter

The sampling site (41.0464°N, 29.0079°E) is located in the touristic/residential area of Beşiktaş, Istanbul at approximately 4–5 m above the ground on a road with heavy traffic. Potential sources of organic aerosol are continuous heavy road traffic on a 6-lane avenue approximately 10–15 m from the sampling site, road traffic on two bridges connecting the European and Asian sides of the city approximately 2–6 km NE of the sampling site, and continuous shipping emissions from local passenger ferries and large vessels crossing through the Bosphorus strait at approximately 5 km in easterly and southerly directions. Additional possible sources include shipping emissions from the Black Sea and a large industrial district 25 km and 45 km in NE and SE directions, respectively.

Particulate matter samples were collected on pre-combusted (450 °C, 8 h) quartz fiber filters using a Tisch PNY1223 high-volume sampler at an average flow rate of 1.13 m^3/min following the USEPA Method IO-2.1 and according to Flores et al. (2020a). The sampler was equipped with an impactor head to collect 2 PM fractions, fine ($D_p < 2.5$ μm) and coarse ($D_p > 2.5$ μm). Fine PM samples were collected at time resolutions of 2 h during daytime and 12 h during nighttime, while coarse PM samples were collected at time resolutions of 24 h. Concentrations of fine PM samples were averaged at the same time resolution of coarse PM. Immediately after collection, the filter samples were wrapped in aluminum foil, inserted into sealable polyethylene bags, and stored in the dark at −20 °C until analysis. Quartz fiber filters were visually inspected and defective filters were discarded. Field blanks were collected for each sampling campaign to evaluate possible contamination by briefly placing filters on the sampler and sampling zero air volume. Field blanks were treated in the exact same way (i.e., preparation, storage, analysis, etc.) as field samples. The sampler was calibrated with a certified variable orifice meter for each sampling campaign to determine the required operating motor pressure. The total volume of sampled air was calculated for each sample according to average operating motor pressure, ambient air temperature and pressure, and exact sampling time. The average volumes were 138, 860, and 1686 m^3 for fine daytime (i.e., 2 h), fine nighttime (i.e., 12 h), and coarse samples (i.e., 24 h), respectively. Pre-cleaned stainless steel tweezers were used to handle filters at all times.

In order to study inter-year variations, sampling was performed for a total of six weeks within one calendar year between Jan 27, 2017 and Jan 11, 2018. The sampling campaigns were as follows: (1) Jan 26-Feb 4, 2017; (2) Feb 17–23, 2017; (3) May 3–9, 2017; (4) July 6–12, 2017; (5) October 20–26, 2017, and (6) Jan 4–10, 2018; hereby referred to as winter1, winter2, spring, summer, fall, and winter3, respectively.

2.2. Sample analysis

300 fine and 50 coarse filter samples were processed for identification and quantification of 16 PAHs and 28 *n*-alkanes with a thermal desorption-gas chromatography–mass spectrometry (TD-GC–MS) system as explained in detail by Flores and Mertoglu (2020). Briefly, filter pieces corresponding to 1–2 m^3 of sampled air were inserted into pre-cleaned thermal desorption glass tubes containing a small plug of deactivated glasswool at one end. The thermal desorption unit (Unity-xr, Markes International, England) operated at the following conditions: simultaneous sample desorption from the tube at 330 °C for 10 min and sorption on a carbon trap at 0 °C and 50 ml min^{-1}, followed by simultaneous desorption from the carbon trap at 350 °C for 10 min and transfer to the GC–MS through a 2 m heated deactivated fused silica column. The GC–MS (7890B/5877E, Agilent Technologies Inc., United States) was equipped with a DB-5 ms column (30 m × 0.25 mm I.D. × 0.25 μm film thickness, J & W Scientific) and operated at a constant pressure of 17 psi. The GC oven was initially held at 100 °C for 3 min, incrementally increased to 150 °C and 325 °C at 25 °C min^{-1} and 5 °C min^{-1}, respectively, and finally held at 325 °C for 10 min. The MS operated at both scan and selected ion monitoring (SIM) modes at a temperature of 150 °C. For identification, the mass spectra obtained were compared to spectra in NIST libraries and the literature. Unique fragment ions were used to quantify the target analytes according to Flores and Mertoglu (2020). The target analytes included (1) PAHs Acenaphthene (Ace), Acenaphthylene (Acy), Anthracene (Ant), Benz[*a*]anthracene (BaA), Benzo[*a*]pyrene (BaP), Benzo[*b*]fluoranthene (BbF), Benzo[*ghi*]perylene (BghiP), Benzo[*k*]fluoranthene (BkF), Chrysene (Chry), Dibenz[*a,h*]anthracene (DahA), Fluoranthene (Flt), Fluorene (Flu), Indeno[1,2,3-*cd*]pyrene (IP), Naphthalene (Naph), Phenanthrene (Phen), and Pyrene (Pyr), and (2) C_8-C_{40} *n*-alkanes. Naphthalene and C_8-C_{13} were not identified in PM samples. C_{14} was quantified only in winter samples. Concentrations of PAHs and *n*-alkanes in TSP were calculated as the sum of the total concentrations in the fine and coarse fractions.

2.3. Data collection

Concentrations of PM_{10}, CO, NO, and O_3 were provided by the Turkish Ministry of Environment and Urbanization for Beşiktaş station (41.0520°N, 29.0094°E), located 690 m North of our sampling station on the same avenue. Meteorological data (i.e., temperature, pressure, wind direction, wind speed, relative humidity, precipitation rate, and solar radiation) were obtained from weather underground (https://www.wunderground.com) for Balmumcu station (41.0580°N, 29.0169°E) which is 1570 m NE of the sampling station. Mixing coefficient and boundary layer height forecasts at the sampling site coordinates were obtained from the global data assimilation system

(GDAS, 1° × 1° ×, 3 h) operated by National Oceanic and Atmospheric Administration (NOAA)'s air resource laboratory (ARL, http://ready.arl.noaa.gov/READYamet.php). Ventilation coefficients ($m^2\ s^{-1}$) were estimated as the product of boundary layer height (m) and wind speed ($m\ s^{-1}$). Traffic density data (i.e., number of vehicles per unit time) were provided by the department of transportation in Istanbul for sensor No. 263, located approximately 460 m N of the sampling site on the same avenue. Due to technical issues with the sensor, traffic density was not available for spring and summer sampling campaigns. Daily averages were calculated for concentrations of air pollutants and meteorological data, while daily total values were calculated for traffic density for source apportionment studies.

3. Results and discussion

3.1. SVOCs in fine and coarse PM fractions

3.1.1. Seasonality of $PM_{2.5}$ and SVOCs

Fig. 1 shows the seasonal variations of total $PM_{2.5}$ mass, and PAHs and *n*-alkanes in fine and coarse PM samples collected on the various sampling campaigns between Jan 28, 2017 and Jan 11, 2018. Between Jan 1 and Dec 31, 2017, the annual mean concentration of $PM_{2.5}$ mass was 29.1 μg m^{-3} with ranges of 20.7 μg m^{-3} (in summer) to 30.7 μg m^{-3} (in winter), thereby slightly exceeding the European Commission Standard of 25 μg m^{-3}.

The yearly averages of PAHs and *n*-alkanes in the fine fraction were 21.6 ng m^{-3} and 103.8 ng m^{-3}, with seasonal-average ranges of 13.2–45 ng m^{-3} and 77.6–146.1 ng m^{-3}, respectively. The concentrations of PAHs (2.2 ng m^{-3}) and *n*-alkanes (11.9 ng m^{-3}) in the coarse fraction were approximately one order of magnitude lower than in the fine fraction. Overall, concentrations of $PM_{2.5}$, PAHs, and *n*-alkanes in the fine fraction were higher in winter and lower in spring and summer. This is a common trend of air pollutant concentrations in urban areas due to variations in emission sources and meteorology (e.g., (Flores et al., 2020a; Kumar and Yadav, 2016). Concentrations of $PM_{2.5}$ were comparable in fall and winter. This may be due to a combination of emissions from residential heating and a stable atmosphere. On the other hand, PAHs and *n*-alkanes during the fall were comparable to spring and summer. This behavior is likely due to precipitation events (total 14 mm) and higher ventilation coefficients observed during the sampling campaign in the fall (average 790 $m^2\ s^{-1}$) that were similar to spring (average 759 $m^2\ s^{-1}$). During the winter, relatively lower concentrations of PAHs and *n*-alkanes were observed in winter2 compared to winter1 and winter3. This effect may be also associated with precipitation (total 10.4 mm) and a higher boundary layer in winter2 compared to winter1 and winter3 (Table S1, supplementary material). Concentrations in the coarse fraction had similar seasonal variations as those observed in the fine fraction, with the exception of spring. Particularly, average concentrations of *n*-alkanes were higher in spring (12.5 ng m^{-3}) than in winter1 (8.9 ng m^{-3}) and winter2 (9.63 ng m^{-3}). High concentrations of PAHs and *n*-alkanes in spring were associated with shipping emissions NE of the sampling site as shown in Figs. S1c and S1i, respectively.

Table S2 shows a comparison between the concentrations found in this work and other megacities and urban traffic sites. For the comparison, only studies performed in megacities and traffic sites were considered in both the fine and coarse fractions. The SVOC concentrations found in this work were lower than other megacities and traffic sampling sites such as Mexico City (Mexico), Beijing (China), Kolkata (India), and Monterrey (Mexico). However, they were one order of magnitude higher than megacities in the USA (Los Angeles) and Europe (Paris, London), and urban traffic areas such as Incheon (Korea) and Lima (Peru). As shown in Table S2, some regions in China and India have more serious air pollution levels than the ones found in this work. However, the concentrations in this traffic site are much higher than in other regions in the USA and Europe. This indicates the urgent need for the establishment of air pollution control strategies such as traffic control and minimizing the use of coal for residential heating in order to prevent the increase in air pollutant concentrations.

3.1.2. Time series of daily $PM_{2.5}$ and SVOCs

A total of 16 PAH and 28 *n*-alkanes were determined in 300 fine and 50 coarse PM samples in four seasons. Fig. 2 shows the time series of $PM_{2.5}$ and identified SVOCs in the fine and coarse fractions. During the sampling campaigns, the daily concentrations of $PM_{2.5}$ ranged from 12.8 to 97.4 μg m^{-3} and approximately 50% of the days exhibited concentrations higher than the US-EPA standard of 35 μg m^{-3}, especially during the fall and winter. Concentrations in spring were slightly below the limit value and showed an average concentration of 29 μg m^{-3}. In Istanbul, natural contributions to PM concentrations from desert dust are common in spring (Flores et al., 2017). As shown by the BSC-DREAM8b model (Basart et al., 2012), two separate dust transport events were observed prior to and during this sampling campaign (Fig. S2). Concentrations in the summer were well below the standard with ranges between 12.8 and 27.0 μg m^{-3}.

The daily concentrations of PAHs in the fine fraction ranged from 7.1

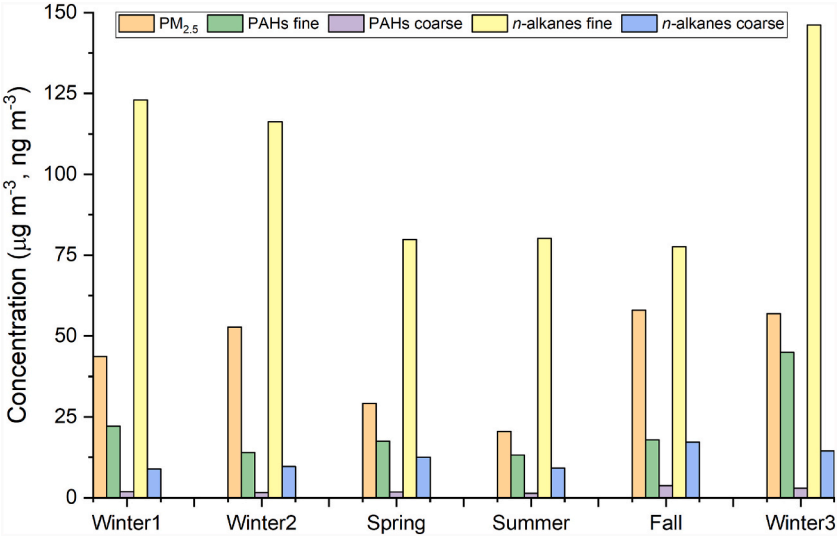

Fig. 1. Average concentrations of $PM_{2.5}$ (μg m^{-3}), and SVOCs (ng m^{-3}) in the fine and coarse fractions during various seasons.

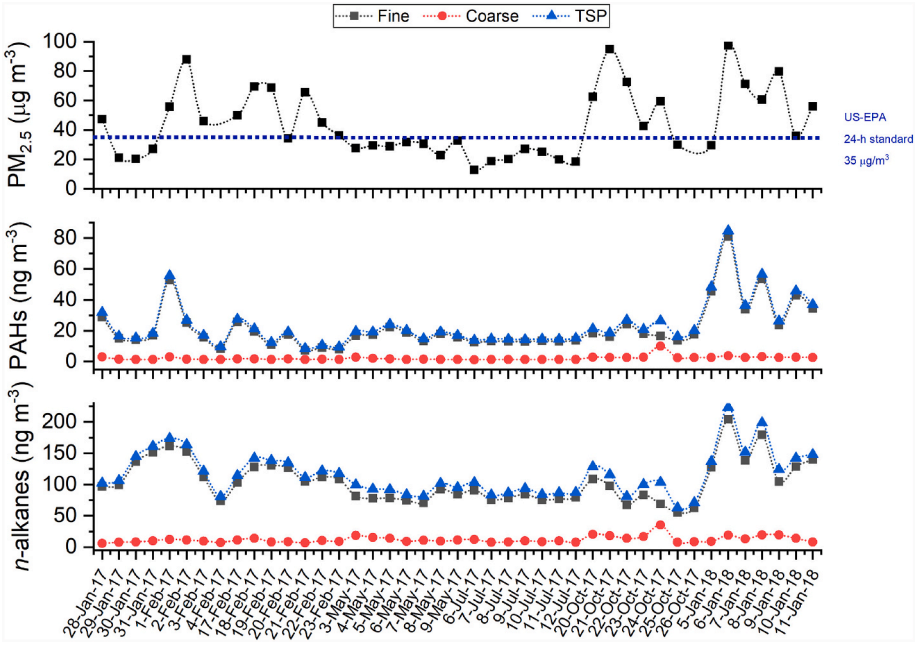

Fig. 2. Daily average concentrations of total $PM_{2.5}$ mass, and PAHs and *n*-alkanes in fine, coarse, and TSP.

to 80.8 ng m^{-3} with annual mean values of 21.6 ± 14.0 ng m^{-3} (Fig. 2). The average PAH concentrations in the TSP fraction (Fig. 2) in fall and winter (i.e., 27.1 ng m^{-3}) found in this work were approximately three times lower than those found by Hanedar et al. (2014) (i.e., 84.6–100.7 ng m^{-3}) in two urban areas of Istanbul in the fall and winter 2007. As expected, the highest concentrations were observed during the winter, due to increased emissions from residential heating and a stable atmosphere. However, significant variations were observed between winter 2017 (i.e., winter1 and winter2) and winter 2018 (i.e., winter3). The average concentration in winter 2017 was 18.0 ng m^{-3}, while in winter3, an average concentration of nearly 45 ng m^{-3} was observed. The main reason for this discrepancy may be related to variations in meteorology. Low wind speeds (1.2 m s^{-1}) and overcast conditions (117.7 W m^{-2}) were observed during winter3 (Table S1). These conditions caused accumulation and hindered the photochemical degradation of SVOCs. This shows the importance of controlling the emissions of air pollutants, particularly during the winter, when meteorology plays an important role in the increase of the concentrations. Fig. 2 also shows the concentrations of PAHs in the coarse fraction. As shown in the figure, the PAHs were primarily distributed in the fine fraction, with averages of 89–93% at all seasons, with the exception of fall (83%). In the fall, the distribution of PAH in the coarse fraction slightly increased to 17%, particularly on 10/24/2017, which had a drastic decrease in solar radiation (Table S1). These results have an important implication on human health since fine particles are respirable and have a longer lifetime in the atmosphere.

The daily concentrations of *n*-alkanes in the fine fraction ranged from 55.3 to 204.2 ng m^{-3} with annual mean values of 104.2 ± 32.7 ng m^{-3} (Fig. 2). The time series of *n*-alkanes showed similar seasonal variations as the PAHs, indicating that the sources may be similar and meteorology variables influence the concentrations in a similar way. Similarly to PAHs, 90–93% of the total *n*-alkane concentrations were distributed in the fine fraction, with the exception of spring (86%) and fall (82%). Overall, PAHs and *n*-alkanes showed more pronounced daily variations in the fine fraction than in the coarse fraction (Fig. 2). This may be due to differences in atmospheric dynamics (e.g., transport, dilution, and transformation) and contributions from different sources. As shown in Table S5, PAHs and *n*-alkanes had a strong Pearson correlation in the fine (R = 0.71) and coarse (R = 0.81) fractions but weak correlation coefficients between fine and coarse fractions. For example, PAHs in the fine fraction and PAHs in the coarse fraction had a Pearson correlation coefficient of 0.33, while *n*-alkanes in the fine fraction and *n*-alkanes in the coarse fraction had a Pearson correlation coefficient of 0.09. The weak correlations between the fine and coarse fractions may indicate contributions from different sources and variations in transport patterns as explained in Section 3.2.

The number of PAH aromatic rings can be used as an indicator for environmental fate, phase distribution, potential sources, and effects on human health (Abdel-Shafy and Mansour, 2016; Choi et al., 2010; Hussain et al., 2018; Wolska et al., 2012). In addition to the physicochemical properties of PAHs, environmental variables such as temperature, relative humidity, and precipitation influence the gas-to-particle partitioning (Hussain et al., 2018). PAHs in the particle phase have various exposure pathways and are considered to be very hazardous to human health since the carcinogenicity prevails for a longer period of time (Abdel-Shafy and Mansour, 2016; Choi et al., 2010). Fig. 3 shows the distribution of PAHs in the (a) fine and (b) coarse fractions according to their number of rings. In this work, the distribution of PAHs in the coarse fraction (Fig. 3b) did not show significant seasonal variations. The main components in the coarse fraction were intermediate-molecular weight PAHs with 4 aromatic rings (18–27%) and high molecular weight PAHs with 5 aromatic rings (46–53%). Heavy PAHs and low MW PAHs represented 25–29% and 0–3% of the total PAH concentration over the whole sampling period, respectively. Similarly to the coarse fraction, PAHs with 4 and 5 aromatic rings were more abundant in the fine fraction with seasonal averages of 32% and 40%, respectively. In the fine fraction, low molecular weight PAHs were found in high amounts in winter1 and winter2 with concentrations 1–2 times higher than in winter3. LMW PAHs are associated with light-duty diesel vehicles and although they are emitted in the gas phase, low ambient air temperature and high relative humidity favor their partitioning into the particle phase (Qin et al., 2021; Ranjan et al., 2012). In the fine fraction, low MW PAHs with 3 aromatic rings represented 4–21% of the total PAH concentration during the various seasons, particularly in winter1 and winter2, which had lower ambient temperature than winter3 (Fig. 3a, Table S1).

3.1.3. *Profiles of individual SVOCs*

The analysis of SVOC profiles is helpful for the understanding of potential sources and effects on human health and the environment.

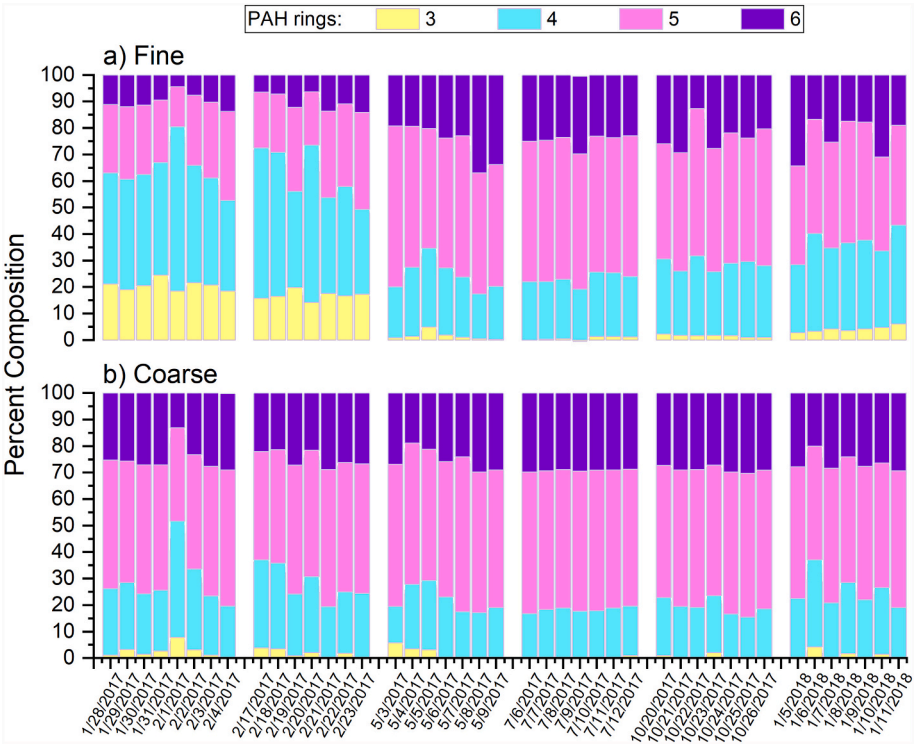

Fig. 3. Distribution of PAHs in a) fine and b) coarse PM fractions.

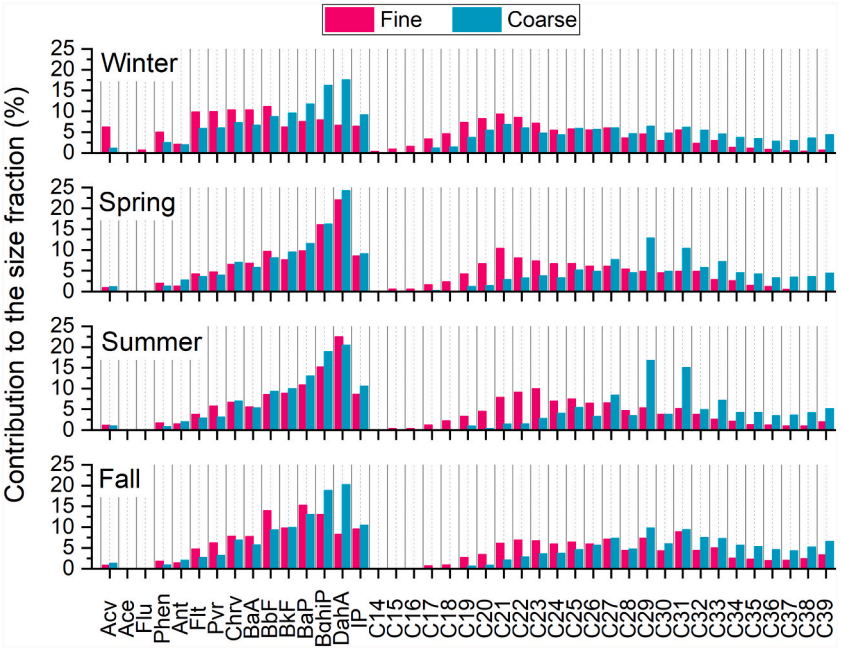

Fig. 4. Abundance (%) of PAHs and *n*-alkanes in the fine and coarse PM fractions.

Figs. 4 and S3 show the seasonal profiles of PAHs and *n*-alkanes in the fine and coarse fractions, both as a percentage contribution to the total size fraction (Fig. 4), and as individual concentrations (Fig. S3). The profiles show that the distributions on the fine and coarse fractions changed according to the SVOC physicochemical properties (i.e., molecular weight, volatility) and according to seasonal variation of meteorological conditions (i.e., ambient air temperature). In general, low molecular weight SVOCs were associated with the fine fraction, whereas high-molecular weight SVOCs were associated with the coarse fraction, with the exception of PAHs in spring and summer. Due to higher ambient air temperatures and evaporation, lower contributions of PAHs with 3 and 4 aromatic rings to the particle phase could be observed in spring and summer. Therefore, both the fine and coarse fractions were mainly composed of PAHs with 5- and 6- aromatic rings.

PAHs with 3 rings Acy, Phen, and Ant contributed to 6.2, 4.9, and 2.1% of the total PAHs in the fine fraction in winter and approximately 1–2% in other seasons. The higher abundance in winter may be due to a combination of lower temperature that causes partitioning into the

particle phase, and the advantage that high-time resolution sampling provides by minimizing negative artifacts due to volatilization losses of SVOCs (Rigler et al., 2020).

The results show that SVOCs were mostly distributed in the fine PM fraction. Concentrations in winter were one order of magnitude higher in the fine fraction than in the coarse fraction. Similarly, concentrations in other seasons were approximately five times higher in the fine fraction than in the coarse fraction (Fig. S3). *n*-alkanes and PAHs have been found preferentially associated with the fine fraction in megacities and other urban areas (Ari et al., 2020; Bi et al., 2005; Tang et al., 2006) and this has important implications on human health and the environment due to the longer lifetimes of fine particles compared to coarse particles.

Similarly to PAHs, *n*-alkanes with low molecular weight (C_{14}-C_{24}) were mainly distributed in the fine fraction, while high molecular weight *n*-alkanes (C_{25}-C_{39}) were mainly distributed in the coarse fraction. In spring and summer, higher concentrations of *n*-alkanes with odd carbon numbers, particularly C_{29} and C_{31} were observed in the coarse fraction, which indicates increased emissions from biogenic sources (Javed et al., 2019b).

The US-EPA (1993) has classified 7 PAHs as probably carcinogenic to humans: (1) 4-ring PAHs Chr and BaA, (2) 5-ring PAHs BbF, BkF, and BaP, and (3) 6-ring PAHs DahA and IP, while BaP is the only PAH classified as a carcinogen to humans by the International Agency for Research on Cancer (IARC). The potential carcinogenic and mutagenic risks were determined with BaP equivalents using toxicity equivalent factor (TEF) and mutagenic equivalent factor (MEF), respectively (Durant et al., 1996; Nisbet and LaGoy, 1992). BaP carcinogenic equivalent (BaP-TEQ) and BaP mutagenic equivalent (BaP-MEQ) concentrations (ng m^{-3}) were calculated for each PAH as the product of the PAH concentration and the TEF or MEF factor. Table 1 shows the TEF and MEF factors and the estimated BaP-TEQ and BaP-MEQ concentrations in the fine fraction for each season. The total BaP-TEQ and BaP-MEQ equivalents were on average 5.5 ± 0.6 and 4.7 ± 0.8 ng m^{-3} in the fine fraction, respectively. The total BaP-MEQ concentrations were higher in fall (5.4 ng m^{-3}) and winter (5.3 ng m^{-3}) than in spring (4.6 ng m^{-3}) and summer (3.6 ng m^{-3}). On the other hand, BaP-TEQ did not show considerable variations among the various seasons. The highest total BaP-TEQ concentration was observed in spring (6.3 ng m^{-3}), particularly due to high concentrations of DahA (3.9 ng m^{-3}) and BaP (1.7 ng m^{-3}). The total BaP-TEQ and BaP-MEQ concentrations were on average 6–7 times higher in the fine fraction than in the coarse fraction.

Large variations of BaP-TEQ concentrations have been found in traffic sites. For example, average concentrations of 0.5–1.0 ng m^{-3}, 10–37 ng m^{-3}, and 15.5–106.0 ng m^{-3} have been found in non-heating and heating seasons in Naples (Italy), Urumqi (China), and Katowice (Poland), respectively (Di Vaio et al., 2016; Kozielska et al., 2015; Simayi et al., 2018). According to the Directive 2004/107/EC, the annual average concentration of PAHs must not exceed 1 ng m^{-3} considering BaP as a marker. On the other hand, the National Ambient Air Quality Standard of China establishes a daily limit of BaP of 2.5 ng m^{-3} (Shen, 2016). In this work, the annual average concentration of BaP (2.18 ng m^{-3}) exceeded the EU target value by a factor of 2. Similarly, with the exception of October 23–25, 2017, the daily BaP standard of 2.5 ng m^{-3} was exceeded on each day during the fall (2.5–4.8 ng m^{-3}) and winter3 (3.3–11.1 ng m^{-3}).

3.2. Source analysis

3.2.1. PAH diagnostic ratios

PAHs are emitted by two main sources: petrogenic and pyrogenic. PAHs of petrogenic origin are emitted at moderate temperatures (100–300 °C) from crude oil and its refined fuels such as kerosene, gasoline, diesel, lubricating oils, and asphalt. Pyrogenic sources emit PAHs at high temperatures (350 °C to more than 1200 °C) during the incomplete combustion of organic matter (i.e., coal, wood, petroleum, etc), fossil fuels in power plants and other industrial activities, garbage, gasoline or diesel fuel in vehicles, and forest fires (Abdel-Shafy and Mansour, 2016; Wolska et al., 2012). The PAH profiles are related to the temperature during formation for each source. PAH diagnostic ratios are helpful for source identification and have been extensively reported in the literature (Ari et al., 2020; Elorduy et al., 2016; Javed et al., 2019a; Tobiszewski and Namieśnik, 2012). However, because PAHs may undergo photochemical reactions in the atmosphere, the diagnostic ratios should be used in sampling sites near the emission sources (Javed et al., 2019b). PAHs emitted by combustion sources (i.e., COMPAH, Flu, Pyr, Chr, BbF, BkF, BaA, BeP, BaP, IP, BghiP) can be used as a first diagnostic ratio to quantify the contribution of combustion sources to the total PAH concentration (Zhang et al., 2016). In this work, the average COMPAH/totalPAH ratios were 0.71 and 0.73 in the fine and coarse fractions, respectively, suggesting a significant contribution from combustion sources.

Table S3 shows the diagnostic ratios used in this work, their source identification according to the magnitudes, references, and the seasonal average values obtained in this work according to PM size fractions. The diagnostic ratios were helpful for discrimination of sources such as petrogenic, pyrogenic, wood and coal combustion, gasoline and diesel vehicle exhaust, and road dust. As shown in the table, petrogenic sources were not identified by any of the diagnostic ratios and PAHs in both size fractions were emitted by pyrogenic sources. Ratios such as Ft/(Ft + Pyr) and BaA/(BaA + Chr) identified vehicular emissions as the main source of PAHs. While IP/(IP + PghiP), BbFt/BkFt, BaP/BghiP, and Bghi/IP allowed the discrimination of diesel vehicle exhaust as the main

Table 1
Estimated carcinogenic (BaP-TEQ) and mutagenic (BaP-MEF) potential of PAHs in the fine fraction.

			BaP-TEQ (ng m^{-3})				BaP-MEQ (ng m^{-3})			
	TEF	MEF	Winter	Spring	Summer	Fall	Winter	Spring	Summer	Fall
Acy	0.001	0.0006	0.0012	0.0002	0.0001	0.0001	0.0007	0.0001	0.0001	0.0001
Flu	0.001	NR	0.0001	0.0005	0.0005	0.0004	NR	NR	NR	NR
Phen	0.001	NR	0.0011	0.0004	0.0002	0.0003	NR	NR	NR	NR
Ant	0.01	NR	0.0041	0.0024	0.0020	0.0025	NR	NR	NR	NR
Flt	0.001	NR	0.0024	0.0008	0.0005	0.0009	NR	NR	NR	NR
Pyr	0.001	NR	0.0024	0.0009	0.0008	0.0011	NR	NR	NR	NR
Chry	0.01	0.017	0.0289	0.0117	0.0090	0.0144	0.0491	0.0199	0.0154	0.0245
BaA	0.1	0.082	0.2999	0.1241	0.0749	0.1409	0.2459	0.1018	0.0614	0.1156
BbF	0.1	0.25	0.3530	0.1738	0.1166	0.2600	0.8824	0.4345	0.2916	0.6501
BkF	0.1	0.11	0.1695	0.1356	0.1198	0.1775	0.1865	0.1492	0.1318	0.1953
BaP	1	1	2.3947	1.7550	1.4831	2.8241	2.3947	1.7550	1.4831	2.8241
BghiP	0.01	0.19	0.0227	0.0284	0.0207	0.0232	0.4315	0.5394	0.3936	0.4399
DahA	1	0.29	1.3928	3.8804	3.0697	2.0796	0.4039	1.1253	0.8902	0.6031
IP	0.1	0.31	0.2166	0.1530	0.1177	0.1697	0.6715	0.4744	0.3648	0.5260
Total			4.8895	6.2663	5.0149	5.6939	5.2662	4.5997	3.6320	5.3786
Yearly average					5.5 ± 0.64				4.7 ± 0.8	

source. Finally, coal and wood combustion were identified by BaA/BaP and BaP/BghiP during the fall and winter, particularly for PAHs distributed in the fine fraction.

Figs. 5 and 6 show variations of selected diagnostic ratios on a daily basis and the potential sources for PAHs identified in the fine and coarse fractions, respectively. Overall, the figures show more data scattered on the fine fraction than in the coarse fraction, which indicates the contribution of mixed sources. The diagnostic ratios indicate that the main sources of PAHs in the coarse fraction were diesel exhaust and road dust. Both fractions show the predominance of pyrogenic over petrogenic sources, with fossil fuel combustion and diesel exhaust as the main sources. Petrogenic sources were identified by Ft/(Ft + Pyr) values smaller than 0.4 during the summer. On the other hand, wood and coal combustion were identified by Ft/(Ft + Pyr) values greater than 0.5 in winter 1 which had the lowest temperature of all sampling days in winter.

3.2.2. N-alkane diagnostic indices

The contribution of biogenic or anthropogenic sources of *n*-alkanes may be elucidated with diagnostic indices such as carbon preferential index (CPI), plant wax *n*-alkane index (WNA), petrogenic *n*-alkane index (PNA), and carbon number (C_{max}). The indices are defined as the ratios between concentrations of *n*-alkanes based on their carbon number and potential source. Alkanes emitted by petroleum and fossil fuel combustion do not have preferential odd-even carbon numbers and range between C_{14} and C_{22} (Stone et al., 2011). Alkanes with odd-carbon numbers emitted by plant wax are in the range C_{16}-C_{40} (Stone et al., 2011). In this work, CPI ratios were calculated as follows:

$$CPI = \frac{\Sigma C_{odd}}{\Sigma C_{even}} = \frac{\sum_{i=15}^{i=39} C_i}{\sum_{j=14}^{j=38} C_j} \quad (1)$$

$$CPI_{anthr} = \frac{\Sigma C_{odd}}{\Sigma C_{even}} = \frac{\sum_{i=15}^{i=25} C_i}{\sum_{j=27}^{j=39} C_j} \quad (2)$$

$$CPI_{biog} = \frac{\Sigma C_{odd}}{\Sigma C_{even}} = \frac{\sum_{i=27}^{i=39} C_i}{\sum_{j=26}^{j=38} C_j} \quad (3)$$

$$WNA_{odd} = C_i - 0.5(C_{i-1} + C_{i+1}) \quad (4)$$

$$WNA\ (\%) = \frac{\Sigma C_{odd}}{\Sigma C_{total}} = \frac{\sum [WNA]}{\sum_{i=14}^{i=39} C_i} \times 100 \quad (5)$$

$$PNA\ (\%) = 100 - WNA\ (\%) \quad (6)$$

Where CPI represents *n*-alkanes with odd and even carbon numbers in the homologous series, while CPI_{anthr} and CPI_{biog} discriminate the influence of anthropogenic and biogenic sources, respectively. WNA_{odd} is the concentration of *n*-alkanes with odd carbon number in the homologous series associated with biogenic sources, while WNA (%)

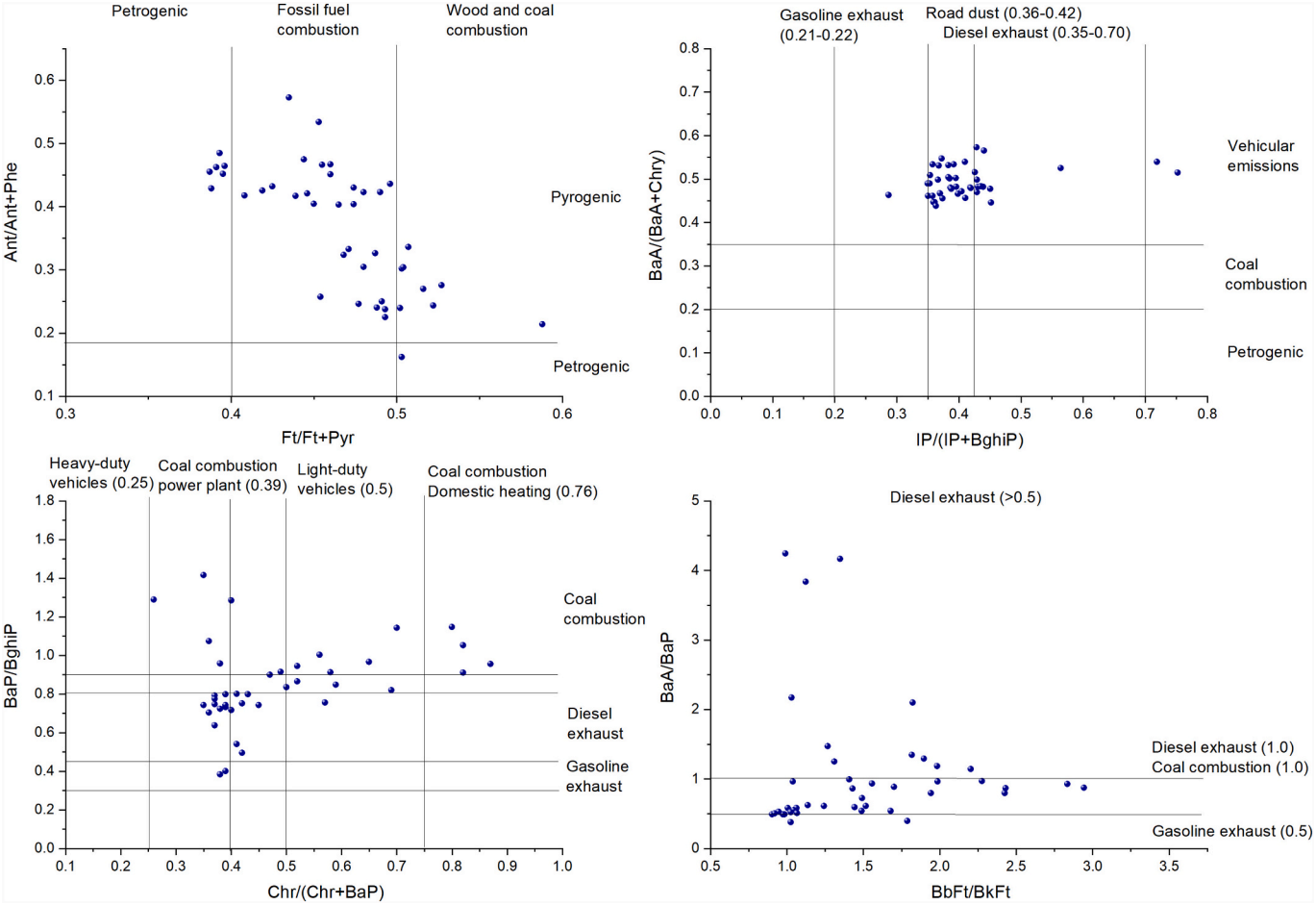

Fig. 5. PAH diagnostic ratios in the fine PM fraction.

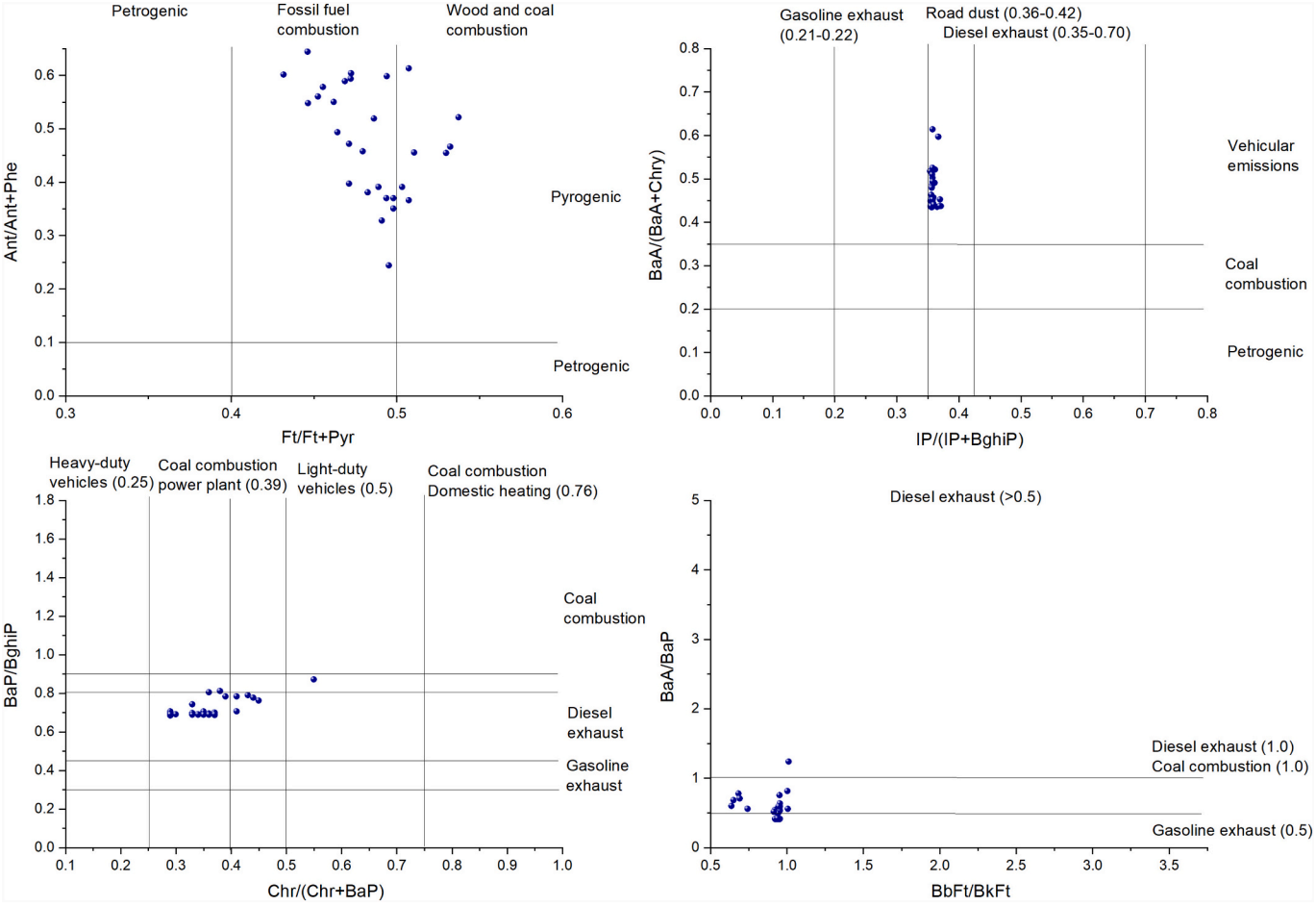

Fig. 6. PAH diagnostic ratios in the coarse PM fraction.

indicates the relative contribution of plant wax to the total concentration (i.e., both odd and even) of *n*-alkanes. Negative WNA values in Eq. (4), were not considered for the estimation of WNA (%) in Eq. (5).

The overall contribution of biogenic sources to the concentrations of *n*-alkanes increases with the magnitude of the CPI ratios. CPI values close to unity indicate the predominance of petroleum emissions, diesel vehicle exhaust, fly ash, etc. while CPI values greater than 1 indicate a strong contribution from biogenic sources such as plant waxes, leaf shedding, pollination, flowering, etc. In this work, CPI values (Eq. (1)) were near 1 in the fine fraction throughout all of the seasons, with a yearly average of 1.2 ± 0.1 (Table S4), indicating a larger contribution from fossil fuel combustion to the fine fraction of the aerosol. In the coarse fraction, CPI values were greater than 1, especially in the summer (2.3), with a yearly average of 1.5 ± 0.4, which is consistent with a larger contribution of biogenic sources due to (e.g.,) plant wax aerosol generated from mechanical abrasion. CPI_{anthr} and CPI_{biog} are useful to determine the contribution of anthropogenic and biogenic sources to the C_{15}-C_{23} (Eq. (2)) and C_{25}-C_{39} (Eq. (3)) *n*-alkane concentrations, respectively. In our traffic sampling site, CPI_{anthr} did not show significant seasonal variations between the fine and coarse fractions, with values of 1.0 ± 0.0 and 0.9 ± 0.1 respectively. Overall, it is observed that *n*-alkanes with less than C_{23} were preferentially emitted by fossil fuel combustion, while a small contribution from biogenic sources was observed for *n*-alkanes greater than C_{23}. CPI_{biog} showed a more significant seasonal variation in the coarse fraction than in the fine fraction, with CPI values twice as large in the summer than in the winter seasons. This observation is also consistent with WNA, which shows that approximately 53% of the total *n*-alkane concentrations in the coarse fraction originated from biogenic sources during the summer, while 15% in the winter. On the other hand, 81% of the total *n*-alkane concentrations in the fine fraction were emitted by anthropogenic sources (Table S4).

The determination of the most abundant *n*-alkane (C_{max}) helps identify the potential main emission source. C_{max} with a carbon number smaller than C_{25} may indicate vehicular exhaust, while C_{max} with a preference for odd carbon numbers greater than C_{27}, with a predominance for C_{29} and C_{31}, are indicators of plant wax (Ari et al., 2020; Gupta et al., 2016). *n*-alkane C_{29} has also been associated with road dust with a mixture of deposited vehicular emissions and plant detritus (Ari et al., 2020). In this work, C_{max} showed a significant predominance for a low carbon number (i.e., C_{21}-C_{27}), particularly in the fine fraction, indicating the potential contribution of vehicular emissions. C_{max} in the coarse fraction showed a predominance for a large carbon number (i.e., C_{29}), indicating the strong contribution from road dust and biogenic sources. Although significant contributions from biogenic sources were determined with these diagnostic indices, *n*-alkane concentrations in the coarse fraction were over one order of magnitude lower than in the fine fraction (Fig. 2). Therefore, minimizing emissions from anthropogenic sources, particularly in traffic sampling sites is of utmost importance due to their effects on human health, atmospheric chemistry, and climate.

3.2.3. *Bivariate polar plots*

In order to identify potential sources of PAHs and *n*-alkanes in both fractions, conditional bivariate probability function plots (CBPF) were created with openair, an open-source package in R (Uria-Tellaetxe and Carslaw, 2014). PAH concentrations were separated into fractions according to the number of rings (i.e., 3–6). Figs. 7 and 8 show the CBPFs in the fine and coarse fractions, respectively. PAHs and *n*-alkanes show a

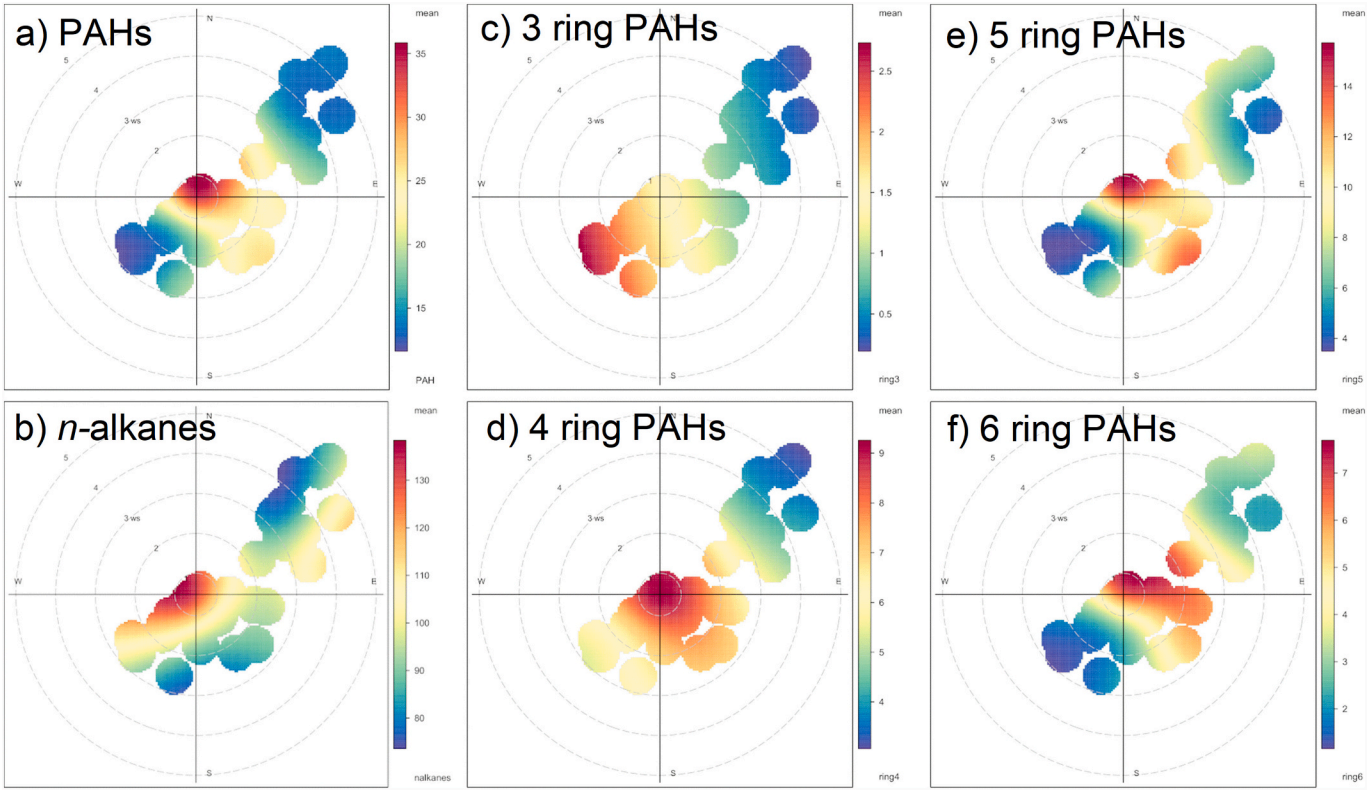

Fig. 7. Polar plots of SVOCs in the fine PM fraction.

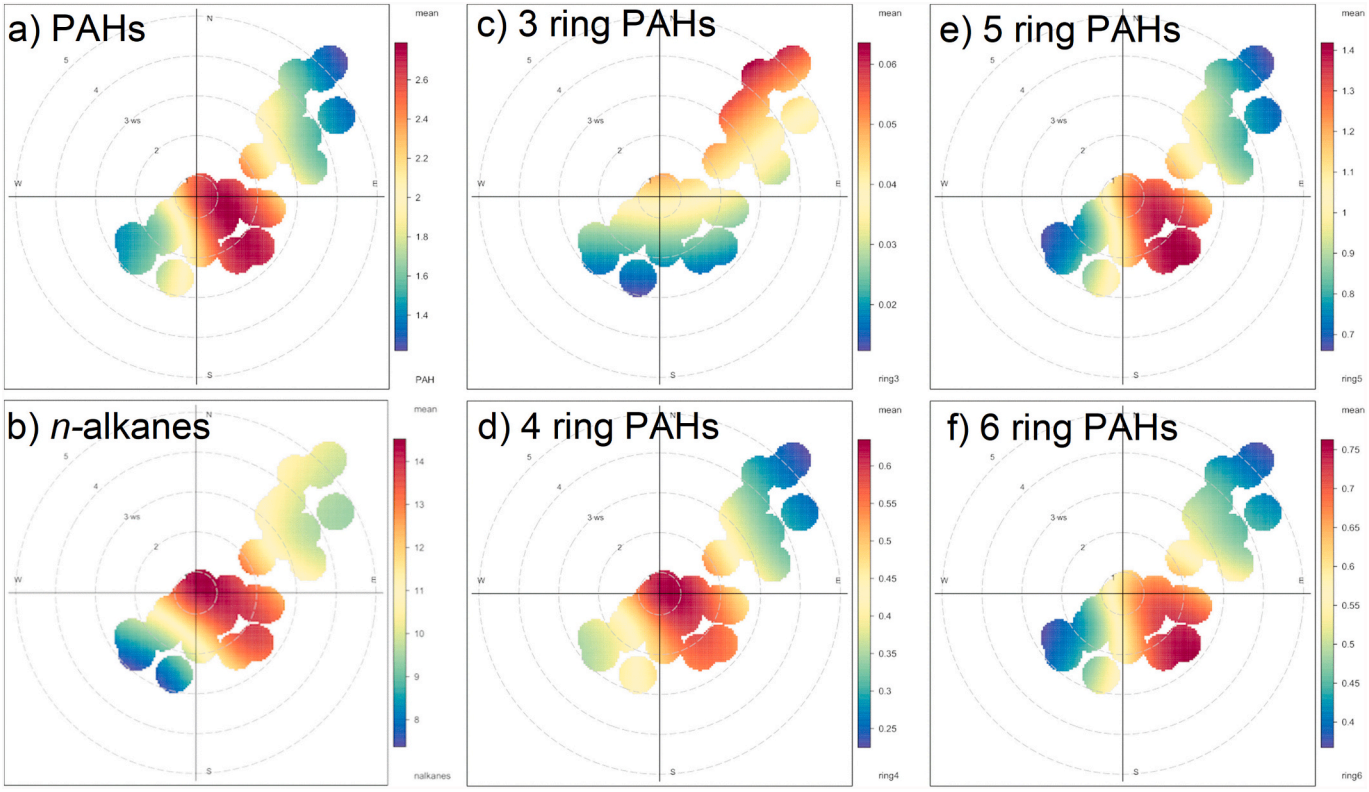

Fig. 8. Polar plots of SVOCs in the coarse PM fraction.

distinct variation in their sources according to the size fraction. Overall, the majority of PAHs and *n*-alkanes in the fine fraction were emitted near the sampling site during stable conditions or episodes with wind speeds lower than 1 m s^{-1}. In the coarse fraction, high concentrations of PAHs and *n*-alkanes showed transport from shipping emissions with easterly winds lower than 3 m s^{-1}. According to the number of rings, a fraction of low molecular weight PAHs (i.e., 3 rings) was transported from the SW direction in the fine fraction and NE direction in the coarse fraction. On the other hand, high molecular weight PAHs (i.e., 4–6 rings) showed similar transport from nearby sources at calm conditions and shipping emissions (i.e., easterly direction) at wind speeds lower than 3 m s^{-1} on both fractions. Similar plots were obtained for black carbon (BC) and nitrogen oxides (NO_x) in a traffic site in Istanbul. In their study, Şahin et al. (2020) found the highest concentrations of traffic-related air pollutants near the sampling site at wind speeds lower than 2 m s^{-1}, which is consistent with road traffic emissions. The results found in this study are also consistent with Flores et al. (2020b) and Şahin et al. (2020), who found that in addition to the contribution from emission sources near the sampling site, EC and BC concentrations were transported from shipping emissions located NE of the sampling site at high wind speeds of 6 m s^{-1} and 4 m s^{-1}, respectively.

3.3. Source apportionment with principal component analysis

Factor analysis was performed with OriginPro 2018 v.9.5.1.195 (OriginLab Co., Northampton, MA, USA). The variable matrix was composed of total concentrations of PAHs and *n*-alkanes in both PM fractions, OC/EC concentrations in the fine fraction (Flores et al., 2020a), PM_{10}, O_3, NO, CO, and SO_2 concentrations, traffic density, and meteorological conditions (temperature, wind direction, pressure, and mixing coefficient). The input variables were determined by an initial analysis of the Pearson correlation matrix (Table S5). Due to the differences in the magnitudes, the variables were normalized by their highest value (e.g., (Chen et al., 2020)). Overall, five factors with eigenvalues higher than unity, with the exception of factor 5 which had an eigenvalue of 0.9, resolved 82.6% of the total variance of the data. The extracted coefficients are shown in Table 2.

The results show that on-road vehicles and local transport of air pollutants contributed to 50.4% and 26.6% of the total concentration of the PAHs and *n*-alkanes in both fractions, respectively (Table 2). An additional factor was interpreted as coal or wood combustion for residential heating with a contribution of 5.6%. PAHs and *n*-alkanes in the fine fraction were associated with OC, traffic-emitted gases CO, NO, and SO_2, and traffic density in Factor 1 (40%). The mixing coefficient had a moderate inverse contribution to Factor 1, which is an indicator for an increase of concentrations during stable conditions in the atmosphere. PAHs and *n*-alkanes have been mainly found in the fine fraction (i.e., $PM_{1.5}$). Particularly near road traffic emissions, they have been associated with particles with diameters smaller than 0.49 μm (Bi et al., 2005). In addition to CO, NO_x, VOCs, and PM, on-road vehicles emit SO_2, particularly diesel vehicles operating with low quality of fuel (Reşitoğlu et al., 2015; Zhao et al., 2010). Similarly to Factor 1, PAHs and *n*-alkanes in the coarse fraction were associated with traffic density in Factor 3 (10.4%). Pressure had a moderate contribution to this factor, which may be an indicator for an increase in the concentrations during episodes with high-pressure systems and a stagnant atmosphere due to sources near the sampling site. The results found in this work are comparable to Hanedar et al. (2014) who found vehicle emissions as the main source of PAH concentrations in the TSP fraction with contributions of 61.2–63.3% in two urban areas in Istanbul.

Factors 2 and 4 were attributed to the transport of air pollutants from nearby sources. Factor 2 (17.6%) had high correlations between PAHs and *n*-alkanes in the coarse fraction and EC concentrations. Temperature and pressure had moderate direct and inverse correlations with PAHs and *n*-alkanes in the coarse fraction and EC, which could be indicators for an increase in the concentrations with ambient temperature, which promotes an increase in the boundary layer height, while a decrease in the ambient pressure promotes horizontal motion of air and transport. Factor 4 (9.0%) was mainly composed of PAHs and *n*-alkanes in the fine fraction, a fraction of *n*-alkanes in the coarse fraction, and EC concentrations. Similarly to Factor 2, in Factor 4, ambient pressure and wind direction had an effect on the concentrations, for this reason, this factor was also attributed to transport from nearby sources.

PAHs and *n*-alkanes in the fine fraction showed strong Pearson correlation coefficients (Table S5) with SO_2 (i.e., $R = 0.59–0.72$) considering the data from all seasons, which may indicate an additional source from coal or wood combustion during the fall and winter seasons (i.e., $R = 0.53–0.67$). The region near the sampling site has a natural gas line used for residential heating. Factor 5 has strong associations between SO_2, mixing coefficient, and pressure, which indicate the possible transport of SO_2 emitted by residential heating activities from nearby areas. However, this factor has a lower contribution to the total variance of the data (i.e., 5.6%) and did not show strong associations with PAHs and *n*-alkanes. Future work with additional source apportionment models with a larger data set including high-time resolved data will be necessary to investigate the influence of possible sources during various seasons.

These source apportionment results are consistent with source analysis performed with CBPF plots (Figs. 7 and 8) showing that the majority of PAHs and *n*-alkanes in both fractions originated near the sampling site due to road traffic emissions (i.e., Factors 1 and 3). Figs. 7 and 8 also show that a fraction of PAHs and *n*-alkanes in both fine and coarse fractions were transported from the easterly direction due to shipping emissions (i.e., Factors 2, and 4). Factors 1, 4 (i.e., road traffic) and Factors 2, 3 (i.e., transport) show high correlations with OC and EC concentrations, respectively. Fig. S4 in supplementary material shows CBPF plots for OC and EC concentrations. As shown in the figures, OC concentrations were mainly emitted near the sampling site, while EC concentrations were also emitted by shipping emissions and transported from NE and E directions. Overall, these results show that variations in emission sources and meteorology have significant effects on the concentrations of organic aerosol and urge the metropolitan authorities to establish measurements to decrease emissions from road traffic and ships to minimize the exposure of the general population and tourists to high levels of air pollutants.

Table 2
Extracted principal components and their loading coefficients.

	Factor 1	Factor 2	Factor 3	Factor 4	Factor 5
	On-road vehicles	Local transport	On-road vehicles	Local transport	Residential heating
PAHs fine	**0.28**	0.27	−0.03	**−0.29**	0.08
n-alkanes fine	**0.34**	0.04	−0.06	**−0.28**	0.07
PAHs coarse	0.09	**0.31**	**0.53**	0.23	0.11
n-alkanes coarse	0.10	**0.37**	**0.42**	**0.32**	0.09
OC	**0.33**	0.24	0.01	−0.10	−0.10
EC	−0.03	**0.42**	0.07	**−0.47**	−0.20
PM_{10}	0.25	0.11	−0.16	**0.40**	−0.25
O_3	0.02	**−0.42**	**0.44**	−0.10	−0.25
NO	**0.32**	−0.10	−0.24	0.24	0.12
CO	**0.33**	0.17	−0.25	0.07	0.04
SO_2	**0.31**	−0.08	−0.14	−0.09	**0.30**
Temperature	−0.27	**0.27**	−0.12	0.13	−0.05
Wind direction	0.25	**−0.27**	0.02	0.26	0.03
Pressure	0.18	−0.23	0.26	**−0.34**	**0.35**
Traffic density	**0.30**	−0.14	**0.30**	0.07	−0.08
Mixing coefficient	−0.23	0.08	0.00	0.10	**0.75**
Percentage of variance	40.0	17.6	10.4	9.0	5.6
Cumulative variance					**82.6%**

4. Conclusions

16 PAHs and 28 *n*-alkanes were determined in fine ($PM_{2.5}$) and coarse ($PM_{>2.5}$) particulate matter collected on selected days throughout all seasons in one calendar year at a traffic site in the megacity of Istanbul for the first time. Seasonal variations with high concentrations in fall/winter and lower concentrations in spring/summer were attributed to variations in emission sources and meteorology. It was found that PAHs and *n*-alkanes were preferentially associated with the fine fraction throughout all seasons, particularly in winter. Overall, the concentrations found in this work were lower than those found in the megacities and urban/traffic areas of Mexico, China, and India but approximately one order of magnitude higher than those found in a USA megacity and other urban areas in Europe.

Heavy PAHs with 4 and 5 aromatic rings showed the highest abundance in both PM fractions, while low molecular weight PAHs with 3 aromatic rings were found in the fine fraction during the winter. The BaP toxicity (BaP-TEQ) and mutagenic (BaP-MEQ) equivalents were on average 5.47 ± 0.64 and 4.72 ± 0.8 ng m^{-3} in the fine fraction, respectively, and were approximately 6–7 times lower in the coarse fraction. Various methods were used for source analysis. PAH diagnostic ratios identified vehicular emission, particularly diesel, as the main source, and coal or wood combustion during the winter. Petrogenic sources were not identified near this sampling site. *n*-alkane diagnostic indices indicated a larger contribution from fossil fuel combustion in the fine fraction, while the contribution from plant wax aerosol was identified in the coarse fraction in summer. Overall, 81% of the total *n*-alkane concentrations in the fine fraction was found to be emitted by anthropogenic sources throughout the whole study period.

Source apportionment with principal component analysis identified traffic emissions (50.4%) and local transport (26.6%) as the main contributions to the total PAH and *n*-alkane concentrations in both fractions. These results were also confirmed by bivariate polar plots, which in addition to traffic emissions near the sampling site, identified transport of shipping emissions with easterly winds. Overall, these results show that variabilities in emission sources and meteorology have significant impacts on the concentrations of organic aerosol and urge the metropolitan authorities to establish control strategies to decrease emissions from road traffic and ships.

Declaration of Competing Interest

The authors declare that they have no known competing financial interests or personal relationships that could have appeared to influence the work reported in this paper.

Acknowledgments

The authors would like to thank the financial support provided by the Scientific and Technological Research Council of Turkey (TÜBITAK) through project No. 115Y625 and Marmara University through project No. FEN-C-DRP-110718-0398. The authors thank IETT-Beşiktaş for use of their facilities, and the Ministry of Environment and Urbanization, and the Department of Transportation for the data provided. Meteorological data were obtained from Weather Underground.

Appendix A. Supplementary data

Supplementary data to this article can be found online at https://doi.org/10.1016/j.atmosres.2022.106100.

References

Abdel-Shafy, H.I., Mansour, M.S.M., 2016. A review on polycyclic aromatic hydrocarbons: source, environmental impact, effect on human health and remediation. Egypt. J. Pet. 25, 107–123. https://doi.org/10.1016/j.ejpe.2015.03.011.

An, Z., Huang, R.-J., Zhang, R., Tie, X., Li, G., Cao, J., Zhou, W., Shi, Z., Han, Y., Gu, Z., Ji, Y., 2019. Severe haze in northern China: a synergy of anthropogenic emissions and atmospheric processes. Proc. Natl. Acad. Sci. U. S. A. 116, 8657–8666. https://doi.org/10.1073/pnas.1900125116.

Ari, P.E., Ari, A., Dumanoğlu, Y., Odabasi, M., Gaga, E.O., 2020. Organic chemical characterization of size segregated particulate matter samples collected from a thermal power plant area. Environ. Pollut. 262, 114360 https://doi.org/10.1016/j.envpol.2020.114360.

Basart, S., Pérez, C., Nickovic, S., Cuevas, E., Baldasano, J., 2012. Development and evaluation of the BSC-DREAM8b dust regional model over Northern Africa, the Mediterranean and the Middle East. Tellus B 64, 18539. https://doi.org/10.3402/tellusb.v64i0.18539.

Bi, X., Sheng, G., Peng, P.A., Chen, Y., Fu, J., 2005. Size distribution of n-alkanes and polycyclic aromatic hydrocarbons (PAHs) in urban and rural atmospheres of Guangzhou, China. Atmos. Environ. 39, 477–487. https://doi.org/10.1016/j.atmosenv.2004.09.052.

Chen, G.-F., Lai, C.-H., Chen, W.-H., 2020. Principal Component Analysis and Mapping to Characterize the Emission of Volatile Organic Compounds in a typical Petrochemical Industrial Park. Aerosol Air Qual. Res. https://doi.org/10.4209/aaqr.2019.07.0365.

Choi, H., Harrison, R., Komulainen, H., Saborit, J.M.D., 2010. Polycyclic aromatic hydrocarbons. In: WHO Guidelines for Indoor Air Quality: Selected Pollutants. World Health Organization.

Di Vaio, P., Cocozziello, B., Corvino, A., Fiorino, F., Frecentese, F., Magli, E., Onorati, G., Saccone, I., Santagada, V., Settimo, G., Severino, B., Perissutti, E., 2016. Level, potential sources of polycyclic aromatic hydrocarbons (PAHs) in particulate matter (PM10) in Naples. Atmos. Environ. 129, 186–196. https://doi.org/10.1016/j.atmosenv.2016.01.020.

Durant, J.L., Busby, W.F., Lafleur, A.L., Penman, B.W., Crespi, C.L., 1996. Human cell mutagenicity of oxygenated, nitrated and unsubstituted polycyclic aromatic hydrocarbons associated with urban aerosols. Mutat. Res. Genet. Toxicol. 371, 123–157. https://doi.org/10.1016/S0165-1218(96)90103-2.

Elorduy, I., Elcoroaristizabal, S., Durana, N., García, J.A., Alonso, L., 2016. Diurnal variation of particle-bound PAHs in an urban area of Spain using TD-GC/MS: influence of meteorological parameters and emission sources. Atmos. Environ. 138, 87–98. https://doi.org/10.1016/j.atmosenv.2016.05.012.

Flores, R.M., Doskey, P.V., 2021. Vapor- and aerosol-phase atmospheric organic matter in urban air of the Midwest USA. Atmos. Environ. 264, 118705 https://doi.org/10.1016/j.atmosenv.2021.118705.

Flores, R.M., Mertoglu, E., 2020. Optimization of a thermal desorption-gas chromatography/mass spectrometry method for characterization of semi-volatile organic compounds in high time resolved PM2.5. Atmos. Pollut. Res. 11, 619–629. https://doi.org/10.1016/j.apr.2019.12.016.

Flores, R.M., Kaya, N., Eşer, Ö., Saltan, Ş., 2017. The effect of mineral dust transport on PM10 concentrations and physical properties in Istanbul during 2007–2014. Atmos. Res. 197, 342–355. https://doi.org/10.1016/j.atmosres.2017.07.009.

Flores, R.M., Mertoğlu, E., Özdemir, H., Akkoyunlu, B.O., Demir, G., Ünal, A., Tayanç, M., 2020a. A high-time resolution study of PM2.5, organic carbon, and elemental carbon at an urban traffic site in Istanbul. Atmos. Environ. 223, 117241 https://doi.org/10.1016/j.atmosenv.2019.117241.

Flores, R.M., Özdemir, H., Akkoyunlu, B.O., Ünal, A., Tayanç, M., 2020b. Seasonal variation of carbonaceous PM2.5 in an Istanbul traffic site. Atmos. Pollut. Res. 11, 2110–2118. https://doi.org/10.1016/j.apr.2020.06.022.

Gupta, S., Gadi, R., Mandal, T.K., Sharma, S.K., 2016. Seasonal variations and source profile of n-alkanes in particulate matter (PM10) at a heavy traffic site, Delhi. Environ. Monit. Assess. 189, 43. https://doi.org/10.1007/s10661-016-5756-7.

Hanedar, A., Alp, K., Kaynak, B., Baek, J., Avsar, E., Odman, M.T., 2011. Concentrations and sources of PAHs at three stations in Istanbul, Turkey. Atmos. Res. 99, 391–399.

Hanedar, A., Alp, K., Kaynak, B., Avşar, E., 2014. Toxicity evaluation and source apportionment of Polycyclic Aromatic Hydrocarbons (PAHs) at three stations in Istanbul, Turkey. Sci. Total Environ. 488–489, 437–446. https://doi.org/10.1016/j.scitotenv.2013.11.123.

Hussain, K., Hoque, R.R., Balachandran, S., Medhi, S., Idris, M.G., Rahman, M., Hussain, F.L., 2018. Monitoring and risk analysis of PAHs in the environment. In: Handbook of Environmental Materials Management, pp. 1–35.

Javed, W., Iakovides, M., Garaga, R., Stephanou, E.G., Kota, S.H., Ying, Q., Wolfson, J. M., Koutrakis, P., Guo, B., 2019a. Source apportionment of organic pollutants in fine and coarse atmospheric particles in Doha. Qatar. J. Air Waste Manage. Assoc. 69, 1277–1292. https://doi.org/10.1080/10962247.2019.1640803.

Javed, W., Iakovides, M., Stephanou, E.G., Wolfson, J.M., Koutrakis, P., Guo, B., 2019b. Concentrations of aliphatic and polycyclic aromatic hydrocarbons in ambient PM2.5 and PM10 particulates in Doha. Qatar. J. Air Waste Manage. Assoc. 69, 162–177. https://doi.org/10.1080/10962247.2018.1520754.

Khare, P., Gentner, D.R., 2018. Considering the future of anthropogenic gas-phase organic compound emissions and the increasing influence of non-combustion sources on urban air quality. Atmos. Chem. Phys. 18, 5391–5413. https://doi.org/10.5194/acp-18-5391-2018.

Khare, P., Machesky, J., Soto, R., He, M., Presto, A.A., Gentner, D.R., 2020. Asphalt-related emissions are a major missing nontraditional source of secondary organic aerosol precursors. Sci. Adv. 6, eabb9785 https://doi.org/10.1126/sciadv.abb9785.

Kozielska, B., Rogula-Kozłowska, W., Klejnowski, K., 2015. Seasonal variations in health hazards from polycyclic aromatic hydrocarbons bound to submicrometer particles at three characteristic sites in the heavily polluted polish region. Atmosphere 6. https://doi.org/10.3390/atmos6010001.

Kumar, P., Yadav, S., 2016. Seasonal variations in water soluble inorganic ions, OC and EC in PM10 and PM>10 aerosols over Delhi: influence of sources and meteorological

factors. Aerosol Air Qual. Res. 16, 1165–1178. https://doi.org/10.4209/aaqr.2015.07.0472.
Kuzu, S.L., Bilgili, L., Kiliç, A., 2021. Estimation and dispersion analysis of shipping emissions in Bandirma Port, Turkey. Environ. Dev. Sustain. 23, 10288–10308.
Lambe, A.T., Onasch, T.B., Croasdale, D.R., Wright, J.P., Martin, A.T., Franklin, J.P., Massoli, P., Kroll, J.H., Canagaratna, M.R., Brune, W.H., Worsnop, D.R., Davidovits, P., 2012. Transitions from functionalization to fragmentation reactions of laboratory secondary organic aerosol (SOA) generated from the OH oxidation of alkane precursors. Environ. Sci. Technol. 46, 5430–5437. https://doi.org/10.1021/es300274t.
Li, J., Han, Z., Li, J., Liu, R., Wu, Y., Liang, L., Zhang, R., 2020. The formation and evolution of secondary organic aerosol during haze events in Beijing in wintertime. Sci. Total Environ. 703, 134937 https://doi.org/10.1016/j.scitotenv.2019.134937.
Li, J., Wang, W., Li, K., Zhang, W., Peng, C., Liu, M., Chen, Y., Zhou, L., Li, H., Ge, M., 2021. Effect of chemical structure on optical properties of secondary organic aerosols derived from C12 alkanes. Sci. Total Environ. 751, 141620 https://doi.org/10.1016/j.scitotenv.2020.141620.
Liu, Y., Li, Y., Yuan, Z., Wang, H., Sha, Q.E., Lou, S., Liu, Y., Hao, Y., Duan, L., Ye, P., Zheng, J., Yuan, B., Shao, M., 2021. Identification of two main origins of intermediate-volatility organic compound emissions from vehicles in China through two-phase simultaneous characterization. Environ. Pollut. 281, 117020 https://doi.org/10.1016/j.envpol.2021.117020.
Ma, P.K., Zhao, Y., Robinson, A.L., Worton, D.R., Goldstein, A.H., Ortega, A.M., Jimenez, J.L., Zotter, P., Prévôt, A.S.H., Szidat, S., Hayes, P.L., 2017. Evaluating the impact of new observational constraints on P-S/IVOC emissions, multi-generation oxidation, and chamber wall losses on SOA modeling for Los Angeles, CA. Atmos. Chem. Phys. 17, 9237–9259. https://doi.org/10.5194/acp-17-9237-2017.
Masiol, M., Hofer, A., Squizzato, S., Piazza, R., Rampazzo, G., Pavoni, B., 2012. Carcinogenic and mutagenic risk associated to airborne particle-phase polycyclic aromatic hydrocarbons: a source apportionment. Atmos. Environ. 60, 375–382. https://doi.org/10.1016/j.atmosenv.2012.06.073.
Molina, L.T., 2021. Introductory lecture: air quality in megacities. Faraday Discuss. 226, 9–52. https://doi.org/10.1039/D0FD00123F.
Nisbet, I.C.T., LaGoy, P.K., 1992. Toxic equivalency factors (TEFs) for polycyclic aromatic hydrocarbons (PAHs). Regul. Toxicol. Pharmacol. 16, 290–300. https://doi.org/10.1016/0273-2300(92)90009-X.
Pandey, P., Patel, D.K., Khan, A.H., Barman, S.C., Murthy, R.C., Kisku, G.C., 2013. Temporal distribution of fine particulates (PM2.5, PM10), potentially toxic metals, PAHs and Metal-bound carcinogenic risk in the population of Lucknow City, India. J. Environ. Sci. Health A 48, 730–745. https://doi.org/10.1080/10934529.2013.744613.
Qin, Y., Ye, J., Ohno, P., Zhai, J., Han, Y., Liu, P., Wang, J., Zaveri, R.A., Martin, S.T., 2021. Humidity dependence of the condensational growth of α-pinene secondary organic aerosol particles. Environ. Sci. Technol. 55, 14360–14369. https://doi.org/10.1021/acs.est.1c01738.
Ranjan, M., Presto, A.A., May, A.A., Robinson, A.L., 2012. Temperature dependence of gas–particle partitioning of primary organic aerosol emissions from a small diesel engine. Aerosol Sci. Technol. 46, 13–21.
Reşitoğlu, İ.A., Altinişik, K., Keskin, A., 2015. The pollutant emissions from diesel-engine vehicles and exhaust aftertreatment systems. Clean Techn. Environ. Policy 17, 15–27. https://doi.org/10.1007/s10098-014-0793-9.
Rigler, M., Drinovec, L., Lavrič, G., Vlachou, A., Prévôt, A.S.H., Jaffrezo, J.L., Stavroulas, I., Sciare, J., Burger, J., Kranjc, I., Turšič, J., Hansen, A.D.A., Močnik, G., 2020. The new instrument using a TC–BC (total carbon–black carbon) method for the online measurement of carbonaceous aerosols. Atmos. Meas. Tech. 13, 4333–4351. https://doi.org/10.5194/amt-13-4333-2020.
Şahin, Ü.A., Onat, B., Akın, Ö., Ayvaz, C., Uzun, B., Mangır, N., Doğan, M., Harrison, R. M., 2020. Temporal variations of atmospheric black carbon and its relation to other pollutants and meteorological factors at an urban traffic site in Istanbul. Atmos. Pollut. Res. https://doi.org/10.1016/j.apr.2020.03.009.
Shen, H., 2016. Global Atmospheric Transport Modeling of benzo[a]pyrene. In: Shen, H. (Ed.), Polycyclic Aromatic Hydrocarbons: Their Global Atmospheric Emissions, Transport, and Lung Cancer Risk. Springer Berlin Heidelberg, Berlin, Heidelberg, pp. 121–137.
Simayi, M., Yahefu, P., Han, M., 2018. Spatiotemporal variation, source analysis, and health risk assessment of particle-bound PAHs in Urumqi, China. Aerosol Air Qual. Res. 18, 2728–2740. https://doi.org/10.4209/aaqr.2018.04.0151.
Stone, E.A., Yoon, S.-C., Schauer, J.J., 2011. Chemical characterization of fine and coarse particles in Gosan, Korea during springtime dust events. Aerosol Air Qual. Res. 11, 31–43. https://doi.org/10.4209/aaqr.2010.08.0069.
Tang, X.L., Bi, X.H., Sheng, G.Y., Tan, J.H., Fu, J.M., 2006. Seasonal variation of the particle size distribution of n-alkanes and polycyclic aromatic hydrocarbons (PAHs) in urban aerosol of Guangzhou, China. Environ. Monit. Assess. 117, 193–213. https://doi.org/10.1007/s10661-006-0440-y.
Tang, J., Li, Y., Li, X., Jing, S.A., Huang, C., Zhu, J., Hu, Q., Wang, H., Lu, J., Lou, S., Rao, P., Huang, D., 2021. Intermediate volatile organic compounds emissions from vehicles under real world conditions. Sci. Total Environ. 788, 147795 https://doi.org/10.1016/j.scitotenv.2021.147795.
Tobiszewski, M., Namieśnik, J., 2012. PAH diagnostic ratios for the identification of pollution emission sources. Environ. Pollut. 162, 110–119. https://doi.org/10.1016/j.envpol.2011.10.025.
Uria-Tellaetxe, I., Carslaw, D.C., 2014. Conditional bivariate probability function for source identification. Environ. Model. Softw. 59, 1–9. https://doi.org/10.1016/j.envsoft.2014.05.002.
US-EPA, 1993. Provisional Guidance for Quantitative Risk Assessment of Polycyclic Aromatic Hydrocarbons (Vol. 600). United States. Environmental Protection Agency. Environmental Criteria & Assessment Office, Ohio. Environmental Criteria and Assessment Office, Office of Health and Environmental Assessment.
Wolska, L., Mechlińska, A., Rogowska, J., Namieśnik, J., 2012. Sources and Fate of PAHs and PCBs in the Marine Environment. Crit. Rev. Environ. Sci. Technol. 42, 1172–1189. https://doi.org/10.1080/10643389.2011.556546.
Yang, L., Zhang, H., Zhang, X., Xing, W., Wang, Y., Bai, P., Zhang, L., Hayakawa, K., Toriba, A., Tang, N., 2021. Exposure to atmospheric particulate matter-bound polycyclic aromatic hydrocarbons and their health effects: a review. Int. J. Environ. Res. Public Health 18, 2177.
Zhang, M., Xie, J., Wang, Z., Zhao, L., Zhang, H., Li, M., 2016. Determination and source identification of priority polycyclic aromatic hydrocarbons in PM2.5 in Taiyuan, China. Atmos. Res. 178-179, 401–414. https://doi.org/10.1016/j.atmosres.2016.04.005.
Zhao, H., Ge, Y., Wang, X., Tan, J., Wang, A., You, K., 2010. Effects of fuel sulfur content and diesel oxidation catalyst on PM emitted from light-duty diesel engine. Energy Fuel 24, 985–991. https://doi.org/10.1021/ef900982c.